ENVIRONMENTAL RESEARCH
LETTERS

ACCEPTED MANUSCRIPT • OPEN ACCESS

Unprecedented mass gain over the Antarctic ice sheet between 2021 and 2022 caused by large precipitation anomalies

To cite this article before publication: Wei Wang *et al* 2023 *Environ. Res. Lett.* in press https://doi.org/10.1088/1748-9326/ad0863

Unprecedented Mass Gain over the Antarctic Ice Sheet between 2021 and 2022 Caused by Large Precipitation Anomalies

Wei Wang[1], Yunzhong Shen[1*], Qiujie Chen[1], and Fengwei Wang[2]

[1] College of Surveying and Geo-informatics, Tongji University, Shanghai, China.

[2] State Key Laboratory of Marine Geology, Tongji University, Shanghai, China.

*Corresponding author: Yunzhong Shen (yzshen@tongji.edu.cn)

Abstract: The Antarctic Ice Sheet (AIS) is susceptible to global climate change, and its mass loss has been 92 ± 18 Gt/yr between 1992 and 2020. Given the current intensive global warming, we investigate the AIS mass changes from January 2003 to December 2022, using the newly released satellite gravimetry and atmospheric datasets. The results show that the continuous mass loss in the AIS between 2003 and 2020 was 141.8 ± 55.6 Gt/yr. However, the AIS showed a record-breaking mass gain of 129.7 ± 69.6 Gt/yr between 2021 and 2022. During this period, the mass gain over the East AIS and Antarctic Peninsula was unprecedented within the past two decades, and it outpaced the mass loss in the Amundsen sector of the West AIS from 2003 to 2022. Basin-scale analysis shows that the mass gain mainly occurred over Wilhelm II Land, Queen Mary Land, Wilkes Land, and the Antarctic Peninsula due to anomalously enhanced precipitation. Further investigation reveals that during 2021–2022, a pair of symmetrically distributed high-low pressure systems, located at approximately 120°W and 60°E in the Southern Ocean, drove the observed abnormal precipitation and mass accumulation.

Keywords: Antarctic Ice Sheet; mass balance; GRACE/GRACE-FO; sea level change; climate change

1 Introduction

The Antarctic Ice Sheet (AIS) melting has the potential to raise the global mean sea level (GMSL) by 58 m, and even a slight sea-level rise has direct societal and economic implications for coastal areas (Oppenheimer et al., 2019; Bars et al., 2017). Therefore, estimating its mass changes and understanding the driving factors is crucial. The AIS mass changes include SMB (surface mass balance) and ice dynamic processes. In the SMB, most ablation is from sublimation, and the important dynamic process is discharge across the grounding line. If the ice mass over the AIS is balanced, snowfall accumulation will balance surface ablation and ice discharge (Rignot et al., 2019). However, numerous reports consistently indicate that the ice mass has been in imbalance, and they concur that ice mass loss over the AIS has outpaced gains from the mid-1990s through 2020 (The IMBIE team, 2018). Specifically, the mass loss over the AIS contributed 7.4 ± 1.5 mm to GMSL from 1992 to 2020 (Otosaka et al., 2022).

Mass changes over the AIS occur from decadal to interannual timescales (Li et al., 2022). The interannual variations affect the estimation of long-term trends (Zhang et al., 2020) and alter the short-term contribution to sea-level changes (Bodart & Bingham, 2019). For instance, 350 Gt net ice gain over Dronning Maud Land (DML) from 2009 to 2011 is assessed by Boening et al. (2012), which is equivalent to a decrease in GMSL rise at a rate of 0.32 mm/yr over the three years. Moreover, relative to the average change from 2002 to 2017, the extreme El Niño event resulted in a mass increase of 277 ± 91 Gt over the AIS between June 2015 and March 2017 (Bodart & Bingham, 2019). The Amundsen Sea sector in the West AIS, the primary source of Antarctic mass loss, experienced a reduction in the total mass loss rate between 2019 and 2020 (Davison et al., 2023). The elevation change records revealed a rapid mass loss in the Amundsen Sea sector from 2003 to 2021, while the mass loss slowed down between 2019 and 2021 (Yue et al., 2023).

Nonetheless, the mass balance over the entire AIS in the recent two years (2021 to 2022) remains unclear. Given the intensive global warming and the impact of Antarctica on GMSL rise, it is imperative to extend the record of mass balance over the AIS and analyze the driving factors behind its short-term mass changes.

During the past decade, the mass balance record over the AIS has been significantly consolidated, benefiting from the data collected by the GRACE (Gravity Recovery and Climate Experiment) mission (Bamber et al., 2018). As a successive mission, GRACE-FO (GRACE Follow-On) tracks changes in gravity since the end of the GRACE mission, allowing quantification of the cumulative mass change between the two missions (Sasgen et al., 2020). With the GRACE and GRACE-FO observations, it has become possible to map the mass changes of the entire Antarctic over longer periods (Velicogna et al., 2020). Therefore, in this study, we analyze the cumulative mass change characteristics over the AIS from January 2003 to December 2022 (20 years) and calculate the biennial mass change rate to demonstrate the short-term mass balance status. Then, we illustrate the geographical patterns of mass change and analyze the direct cause of the mass change. Finally, we reveal the basin-scale interannual mass variation and the primary driving factors.

2 Datasets and processing strategies

2.1 Study area

As defined by Zwally et al. (2012), there are 27 drainage basins over the AIS (Figure 1). These individual basins are then combined into three AIS regions (the IMBIE team, 2018): East AIS (EAIS; Basins 2–17), West AIS (WAIS; Basins 1 and 18–23), and Antarctic Peninsula Ice Sheet (APIS; Basins 24–27).

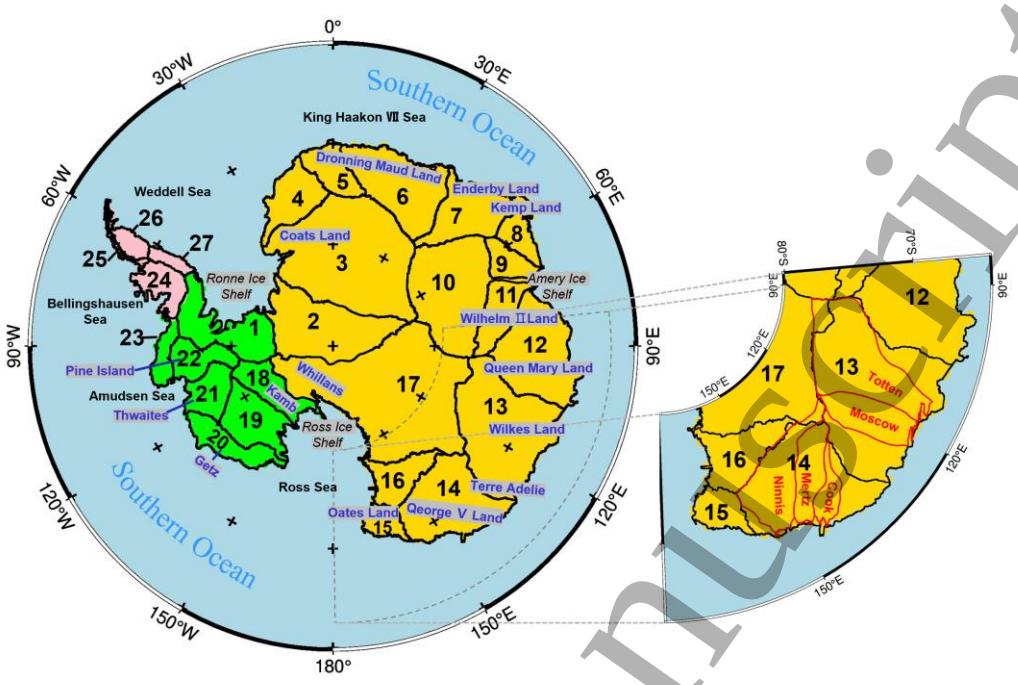

Figure 1. Regional distribution of basins (1–27), with the EAIS colored in light orange, the WAIS in green, and the APIS in pink. Basin boundaries are obtained from Zwally et al. (2012); the glacier and land information are referred to Mouginot et al. (2017) and Cox et al. (2023).

2.2 GRACE/GRACE-FO Data

Using the GRACE/GRACE-FO observations, the mascon (mass concentration) approach can estimate monthly cumulative mass anomalies relative to a given time at specific grid locations on the Earth's surface. Here, we used newly released 0.25 °×0.25° mascon solutions (RL06, version 02) with an extended timespan provided by the CSR (Center for Space Research) at the University of Texas at Austin (Save et al., 2020) to estimate mass changes over the AIS from January 2003 to December 2022. The CSR derives its mascon solutions with spherical harmonic coefficients up to degree and order of 120 (Save et al., 2016) after the C_{20} (degree 2 order 0) coefficients and C_{30} (degree 3 order 0) coefficients for GRACE-FO period are replaced with those from SLR (Satellite Laser Ranging) (Loomis et al., 2019; Loomis et al., 2020) and the absent degree-1 coefficients are

added with those from the Technical Note-13 (Save et al., 2020). The glacial-isostatic adjustment (GIA) correction is completed with the ICE6G-D model (Peltier et al., 2018).

2.3 Meteorological Fields

The Regional Atmospheric Climate Model 2 (RACMO2), Version 2.3p2, with a spatial resolution of 27 km × 27 km, is used to estimate the SMB over the AIS from January 1979 to December 2022 (Van Wessem et al., 2018). Since there are potential errors and biases in particular precipitation datasets (González-Herrero et al., 2023), the average of the precipitation fields from the RACMO2, Modern-Era Retrospective analysis for Research and Applications version 2 (MERRA-2; at 0.5°×0.625° spatial resolution, Gelaro et al., 2017), and the European Centre for Medium-Range Weather Forecasts Reanalysis version 5 (ERA5; at 0.25°× 0.25° spatial resolution, Hersbach & Dee, 2016) reanalysis products is used to explore the relationship between the precipitation and the interannual mass variations over the AIS. The spatial resolutions of the RACMO2 and the precipitation fields are adjusted to match the resolution of CSR mascon solutions through spatial averaging.

2.4 Processing strategies

Since the study period is from January 2003 to December 2022, the cumulative SMB/mass/dynamic anomalies are relative to those in January 2003. Given that RACMO2 provides simulations of absolute SMB, the SMB anomalies are derived by removing their 1979–2008 mean (Rignot et al., 2019; Velicogna et al., 2014). Then, the cumulative SMB anomalies are derived by time-integrating the SMB anomalies from January 2003. Since there is no systematic bias between the GRACE and GRACE-FO time series (Velicogna et al., 2020), the 11-month gap between them is bridged using cumulative SMB anomalies, and the remaining missing data are filled with cubic spline interpolation. Then, the gridded cumulative dynamic mass anomalies are

calculated by removing the cumulative SMB anomalies from the cumulative mass anomalies (Diener et al., 2021). The monthly time series of cumulative anomalies for an individual basin or region is calculated by integrating the values of the grids within the basin or region. The corresponding contribution to GMSL rise is determined by using the relationship that 362.5 Gt mass variation corresponds to 1 mm GMSL change (Cogley et al., 2012). Monthly precipitation anomalies and cumulative precipitation anomalies are derived following the same approach used for RACMO2 SMB. The interannual mass (or precipitation) variation is computed using a 13-month moving average filter on the detrended time series of cumulative anomalies. Consequently, positive interannual mass (or precipitation) variation indicates higher cumulative mass (or precipitation) relative to the mean rate over the study period. In contrast, negative values indicate a reduction in mass (or precipitation).

The long-term mass change trend, or biennial mass change rate (denoted as a in Eq. (1)), is determined by least squares fitting to the time series of cumulative anomalies $M(t)$, using the following equation:

$$M(t_i) = a_0 + a_1 t_i + a_2 \sin(2\pi t_i) + a_3 \cos(2\pi t_i) + a_4 \sin(4\pi t_i) + a_5 \cos(4\pi t_i) \quad (1)$$

where t_i is the ith time tag in years; a_0 and a_0 are the constant and biennial mass change trend (or rate); the last four terms on the right-hand represent the annual and semi-annual signals. The biennial mass change rate calculation employs time series that commence in January of the initial year and conclude in December of the second year. It should be noted that the rates for SMB and dynamic mass change are relative to the average SMB from the reference years 1979–2008.

2.5 Error estimates

The error for the cumulative mass/SMB/dynamic anomaly at a 95% confidence level (or two-sigma) is derived from the law of error propagation based on the fitting error in equation (1),

$$E_{cu(ti)} = 2\sqrt{{\sigma_{a_0}}^2 + {t_i}^2{\sigma_{a_1}}^2 + \sin(2\pi t_i)^2\,{\sigma_{a_2}}^2 + \cos(2\pi t_i)^2\,{\sigma_{a_3}}^2 + \sin(4\pi t_i)^2\,{\sigma_{a_4}}^2 + \cos(4\pi t_i)^2\,{\sigma_{a_5}}^2} \quad (2)$$

where σ_{a_0}, σ_{a_1}, σ_{a_2}, σ_{a_3}, σ_{a_4}, σ_{a_5} are the one-sigma uncertainties for corresponding parameters in equation (1). The error for the mass change trend (or rate) at a 95% confidence level is derived by

$$E_{trend/rate} = 2\sqrt{{\sigma_{a_1}}^2 + {\sigma_{GIA}}^2} \quad (3)$$

where σ_{GIA} denotes the standard deviation of the GIA model, which is empirically calculated by a multimodel comparison as Smith et al. (2020) with six GIA models from A et al. (2013), Ivins et al. (2013), Caron & Ivins (2018), Peltier et al. (2018), Whitehouse et al. (2012), and Sasgen et al. (2018). The errors of the monthly precipitation and cumulative precipitation anomalies are also derived from the three used precipitation fields with the multimodel comparison method.

3 Results and Analysis

3.1 Cumulative mass anomalies and biennial mass change rates between 2003 and 2022

The time series of cumulative mass anomalies and their contribution to GMSL for the AIS, EAIS, WAIS and APIS are depicted in Figure 2 (a–d). Results show that the AIS mass variation experienced a state of near equilibrium from 2003 to 2006, followed by a sustained mass loss until the end of 2020 with a total mass loss of 2552 ± 132 Gt. At the end of 2020, there was a reversal in the mass change state, shifting from loss to gain, which was unprecedented within the past two decades. This reversal reduced the total mass loss to 2083 ± 141 Gt by the end of 2022. In the last

two years, the net mass increase is approximately 469 Gt, counterbalancing a contribution of 1.3 mm to GMSL, which has never been observed since the mid-1990s (Schröder et al., 2019; Otosaka et al., 2023).

Specifically, the EAIS has demonstrated sustained mass accumulation, with particularly pronounced increases from 2009 to 2012, as Boening et al. (2012) and Shepherd et al. (2019) reported. Most strikingly, an even more substantial mass accumulation occurred during 2021–2022 (i.e., from the beginning of 2021 to the end of 2022), and the amount is more significant than that from 2009 to 2012. Conversely, the WAIS continues to lose mass, with a cumulative loss of 3022 Gt until December 2022, contributing to a GMSL rise of approximately 8.4 ± 0.3 mm. Regarding the APIS, two significant mass accumulations occurred during 2015–2016 and 2021–2022. Notably, the mass accumulation during 2021–2022 completely offset the mass loss during 2018–2019, resulting in a seven-year cumulative mass balance from 2016 to 2022. From the cumulative SMB and dynamic mass anomalies, it is obvious that the cumulative SMB directly modulates all the observed sharp mass gains. In contrast, the dynamic mass loss in the WAIS and APIS is the primary source of the total mass loss.

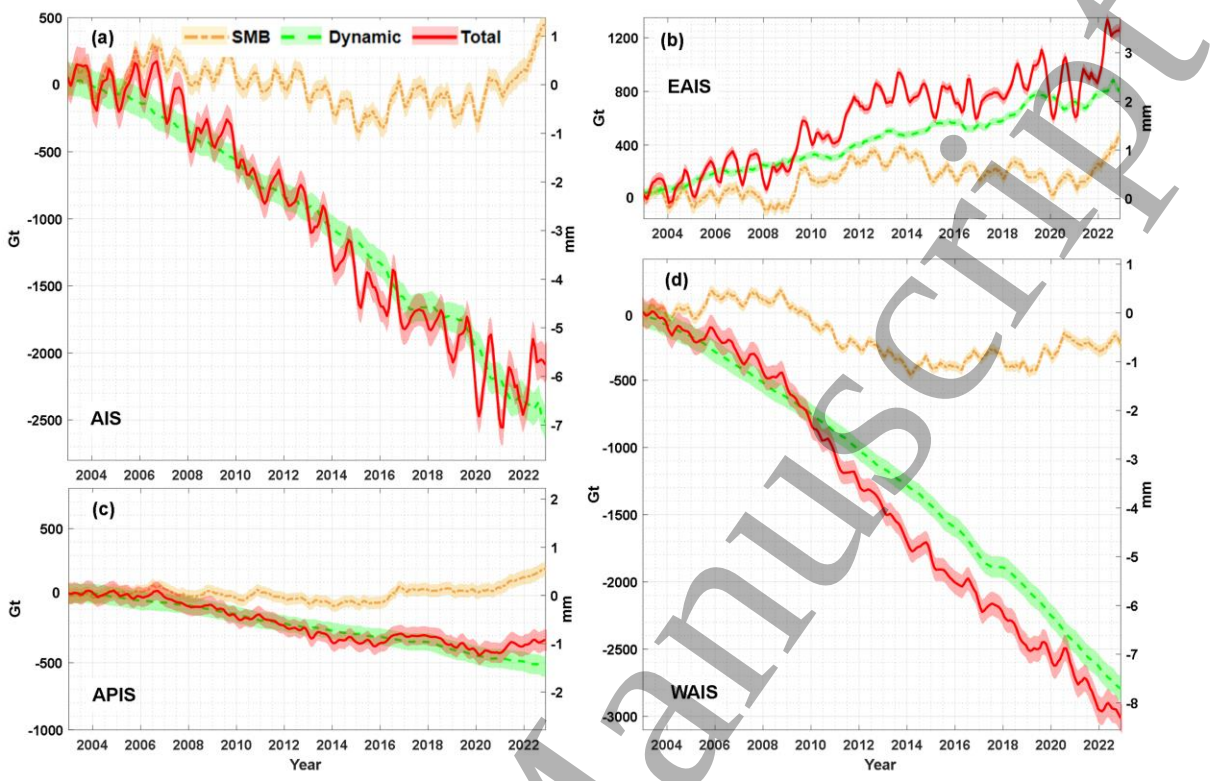

Figure 2. Time series of the cumulative SMB, dynamic, and total mass anomaly relative to January 2003. A 3-month average is applied to the observed total mass anomaly, while a 13-month average is applied to the dynamic mass anomaly to minimize the possible high-frequency noise.

To quantify the short-term mass balance, we calculate the biennial mass change rates between 2003 and 2022 for the AIS, EAIS, WAIS, and APIS, and present them in Figure 3 (a–d). Notably, the AIS exhibited positive mass change rates during 2005–2006 and 2021–2022. In these two biennial periods, there were apparent dynamic mass losses, combined with cumulative SMB gains, particularly evident in 2021–2022. Specifically, the cumulative SMB change at 243.5 ± 29.9 Gt/yr outpaced the ice dynamics mass loss, resulting in a positive rate at 129.7 ± 69.6 Gt/yr. The total mass gain observed during 2021–2022 has never been reported before, and its magnitude of gain is unprecedentedly significant within the past two decades of GRACE/GRACE-FO records.

Notably, there are five biennial mass change rates with clear mass gains over the EAIS between 2003 and 2022, among which the highest mass gain is during 2021–2022, amounting to 273.1 ± 49.1 Gt/yr, more than five times the mass change trend of the EAIS over the past 20 years (52.7 ± 38.8 Gt/yr). The biennial mass change rate of the WAIS is –52.0 ± 32.4 Gt/yr in 2005–2006 and –87.9 ± 21.3 Gt/yr in 2019–2020, roughly equaling one-third and half of the long-term mass loss trend between 2003 and 2020 (165.9 ± 14.8 Gt/yr). Such a reduced amplitude of the mass loss for the WAIS in 2019–2020 has been rare since the late 2010s. The deceleration of mass loss in the WAIS during 2019–2020 is generally consistent with the previously observed slowdown in the Amundsen Sea sector from 2019 to 2021, as indicated by ice sheet elevation changes from multi-altimeter observations (Yue et al., 2023). In the APIS, there was a positive mass change rate in 2015–2016, as Bodart & Bingham (2019) reported. During 2021–2022, the mass change rate again turned positive, and exceeded the previous record of mass gain observed in 2015–2016, reaching an unprecedented large magnitude within the past two decades.

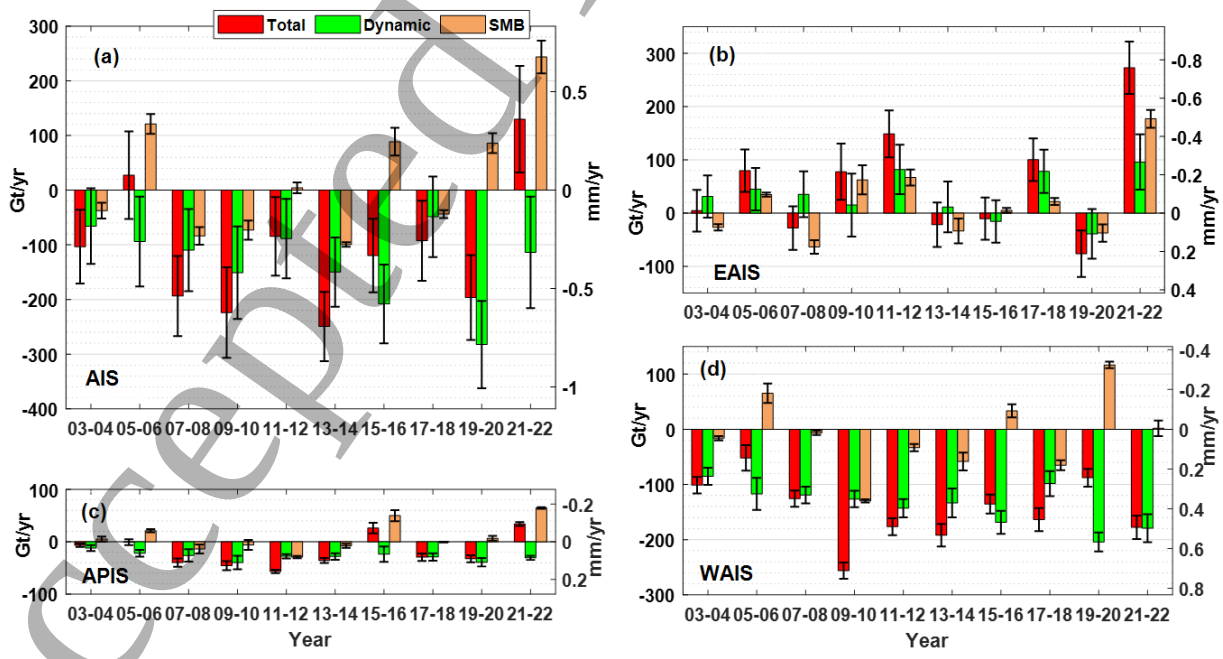

Figure 3. Biennial mass change rates of the total, dynamic mass changes, and cumulative SMB for the AIS, EAIS, WAIS, and APIS between January 2003 and December 2022 (a–d).

3.2 Geographical patterns for mass change trends

To investigate the mass balance before and after the observed mass gain, Figure 4 depicts the geographical patterns of trends from January 2003 to December 2022 and the biennial rates of total mass changes between January 2021 and December 2022. The estimated trends and biennial rates of individual basins for the two periods are shown in Supplementary Table S1, in which Basin 24, 25, 26, and 27 are integrated due to the relatively small area coverage. Additionally, corresponding trends and rates for cumulative SMB/dynamic anomalies are presented to describe the direct cause of total mass change.

From 2003 to 2022, the Amundsen Sea sector and the APIS exhibited clear mass loss patterns. They are primarily driven by ice dynamic imbalances from the fast-flow glaciers of Pine Island, Thwaites, Getz (Rignot, 2014), and several Bellingshausen Sea glaciers, caused by submarine melting (Khazendar et al., 2016; Mouginot et al., 2014) and iceberg calving (Berthier et al., 2012). Besides, the surface mass reduction in the Getz glacier also contributed to the total mass loss though to a lesser extent. Moreover, a prominent mass gain trend is observed in the Kamb ice streams, primarily driven by ice dynamic changes. For the EAIS, the geographical pattern of the mass change trend is more complex. The mass loss trends are evident in Queen Mary Land, George V Land, and Coats Land. In Queen Mary Land, the sustained reduction in cumulative SMB is primarily responsible for these signals. Conversely, in Coats Land and George V Land, the mass losses are predominantly driven by ice dynamic changes from the Totten, Moscow, Cook, Mertz, and Ninnis glaciers. In DML, Enderby Land, and Kemp Land, a widespread pattern of modest ice mass gain extended along much of the coastline and reached several hundred kilometers inland,

closely associated with SMB accumulation. However, ice dynamic losses may offset a small portion of the mass accumulation.

The short-term mass change rates in Figure 4(d–f) provide additional insights for the mass changes in the recent two years. Compared to the past two decades, from 2003 to 2020, the amplitude and even the sign of mass change (gain or loss) between 2021 and 2022 changed significantly over some regions. Most strikingly, there were clear mass loss signals over the APIS from 2003 to 2020. However, during 2021–2022, the mass gain was evident across most regions of the APIS, excluding the narrow peripheral areas in Basin 27. Moreover, there were significant mass gain signals over Basin 12 (Wilhelm II Land and Queen Mary Land) and Basin 13 (Wilkes Land). Basin-scale mass change rates in Table S1 show that Basin 12, 13, and APIS are the top three contributors to the observed 2021–2022 mass gain over the AIS, with the biennial rates of 74.2 ± 8.0 Gt/yr, 63.2 ± 11.6 Gt/yr and 34.1 ± 3.8 Gt/yr respectively. Besides, the mass gain rate over Basin 5–6 (DML) increased twofold from 24.0 Gt/yr to 48.1 Gt/yr. These mass gains are spatially matched with the cumulative SMB change rates, indicating that enhanced SMB accumulation is the direct cause of the observed total mass gain.

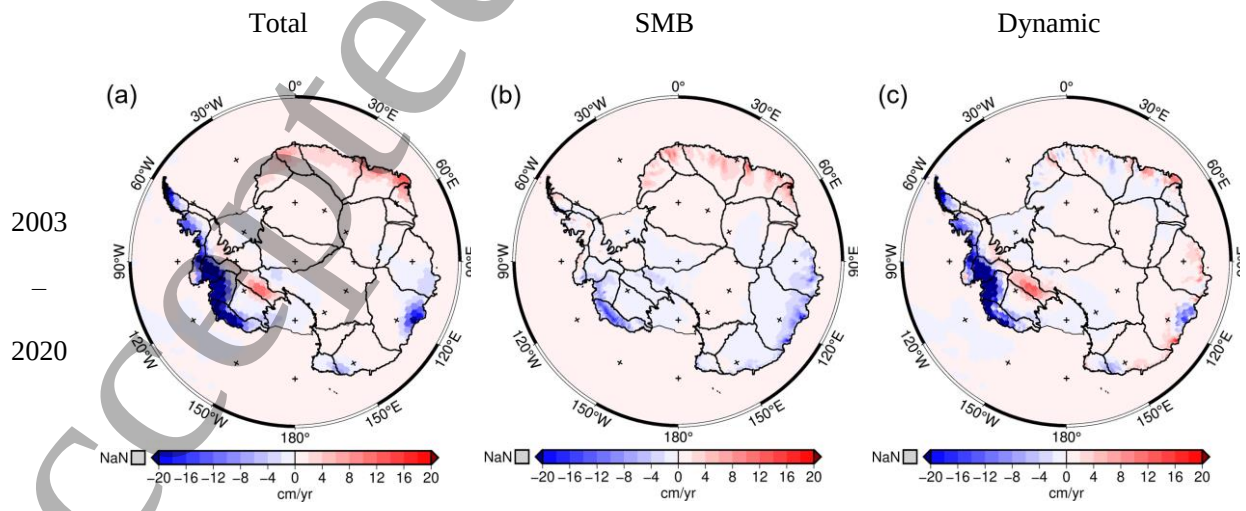

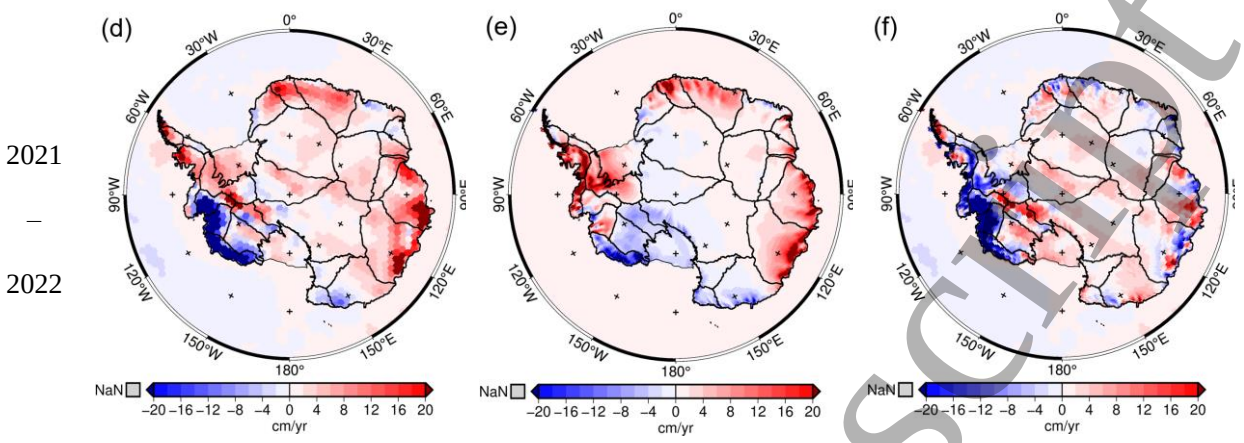

Figure 4. Trends of the total mass change from GRACE/GRACE-FO, cumulative SMB, and dynamic mass anomaly from January 2003 to December 2020 (a–c) and corresponding biennial rates from January 2021 to December 2022 (d–f). The corresponding errors are shown in Supplementary Figure S1.

3.3 Causes for the unprecedented mass gain in the recent two years

To explore the underlying factors of the pronounced interannual variation of cumulative anomalies in total mass over the AIS, especially the observed mass gain in the recent two years, we calculate the interannual variation of cumulative anomalies in total mass and precipitation and derive corresponding cross-correlation coefficients for individual basins. The results for the focused regions of Basin 12, 13, and APIS are shown in Figure 5(a–c).

The cross-correlation coefficients for individual basins over the AIS range from 0.47 to 0.92, with a mean value of 0.75, indicating that the interannual changes in cumulative mass anomalies are primarily driven by cumulative precipitation anomalies (Kim et al., 2020). For Basin 12, 13, and APIS, the interannual variations between cumulative anomalies in precipitation and total mass have a high correlation (Figure 5(a–c)). For Basin 12 (Wilhelm II Land, Queen Mary Land) and Basin 13 (Wilkes Land), the total mass anomalies rapidly accumulated with 361 ± 23 Gt from January 2020 to December 2022, and the contemporary accumulation of precipitation anomalies

was 389 ± 77 Gt. For the APIS, the total mass anomaly increase was 95 ± 47 Gt from May 2015 to December 2017, while the total mass anomaly from July 2020 to December 2022 was 111 ± 54 Gt. The corresponding increases in cumulative precipitation anomalies were 66 ± 31 Gt and 109 ± 83 Gt, respectively. Specifically, for Basin 13, two notably extreme precipitation events in March 2022 and October 2021 (Supplementary Figure S2) accounted for approximately 38% of the total precipitation anomalies over the three years (2020–2022). These two striking precipitation events have been linked to atmospheric rivers (Blanchard-Wrigglesworth et al., 2023; Wille et al., 2023; Clem et al., 2022). For both Basin 12 and APIS, 26 out of 36 months (2020–2022) recorded precipitation levels exceeding the two-decade average (Supplementary Figure S2), indicating that the observed mass anomalies are related to the increased frequency of above-average precipitation.

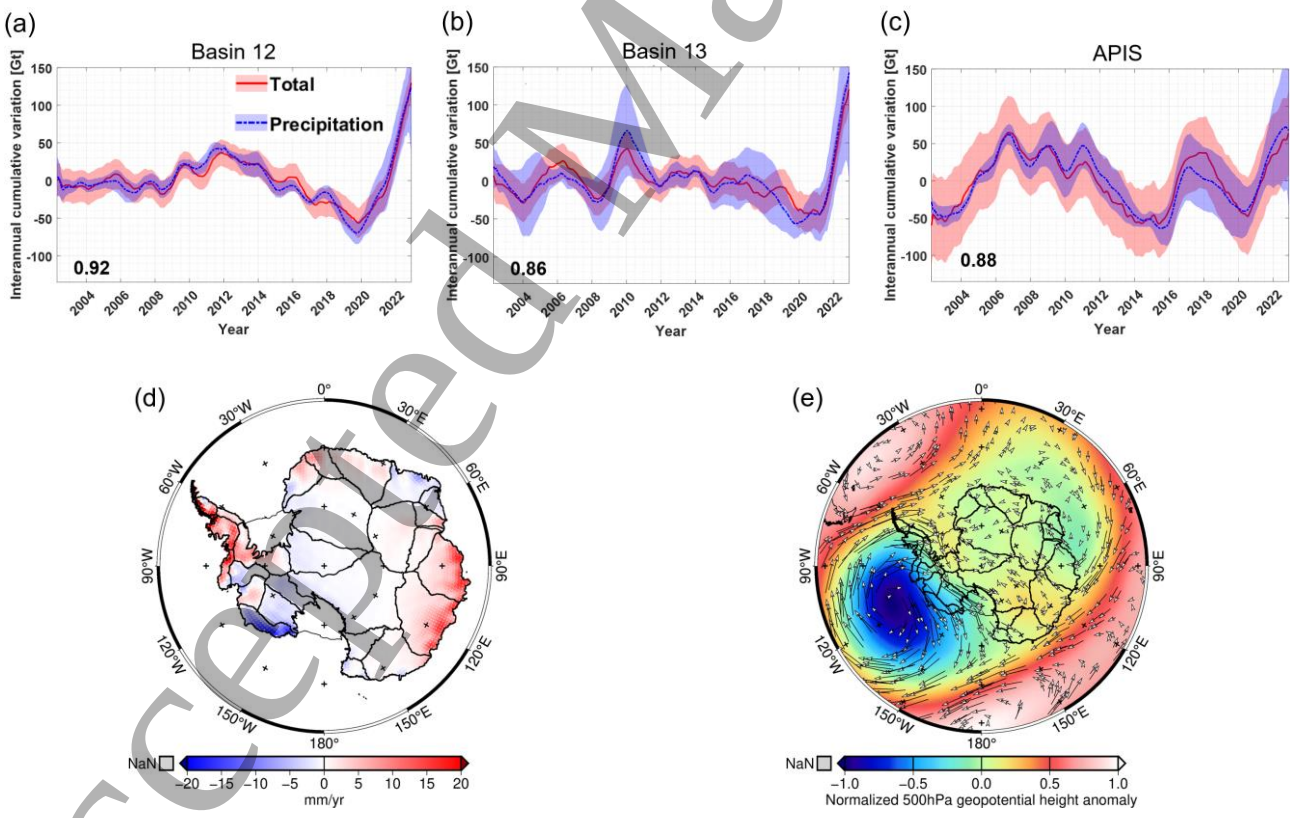

Figure 5. Interannual variations of cumulative anomalies in total mass (red) and precipitation (blue) for basins 12, 13, and APIS (a–c); biennual averaged precipitation anomaly and normalized 500-

hPa geopotential height anomaly for 2021–2022 (d–e), with arrows representing the corresponding wind field anomaly.

As the normalized 500-hPa geopotential height serves as a crucial indicator of atmospheric pressure and motion, we present, in Figure 5 (d–e), the biennial average precipitation anomalies alongside their corresponding anomalies in the normalized 500-hPa geopotential height and wind field from the mean of MERRA-2 and ERA5 for the most recent two years, aiming to investigate the underlying driving mechanism. During 2021–2022, there was a pair of symmetrically distributed high-low pressure systems located at approximately 120°W and 60°E over the Southern Ocean. They altered the direction of the prevailing westerly winds anomalies and resulted in an excessive amount of moisture being transported toward parts of the coastal region of the EAIS, especially Basin 9–11, Basins 12, 13, the APIS, and the DML. This explains the highly enhanced precipitation in the recent two years and the significant mass accumulation depicted in Figure 4 (d–f) and Figure 5 (a–c). The atmospheric pressure change and its motion are essential conduits in the ocean-land mass cycle, facilitating mass transfer from the ocean to land. In other words, the modulation of the interannual mass variations of the AIS is the response to atmospheric forcing (Adusumilli et al., 2021).

4 Conclusions

We quantified the mass change over the AIS from January 2003 to December 2022 using the GRACE/GRACE-FO and atmospheric datasets. We analyzed the biennial mass change rates to demonstrate short-term mass change. The continuous mass loss in the AIS between 2003 and 2020 was 141.8 ± 55.6 Gt/yr. Subsequently, the AIS showed a mass gain of 129.7 ± 69.6 Gt/yr between 2021 and 2022, which was record-breaking within the past two decades of GRACE/GRACE-FO records. During this period, the mass gain over the East AIS and Antarctic Peninsula reached

unprecedented levels within the past two decades, surpassing the mass loss observed in the Amundsen sector of the West AIS. Basin-scale analysis shows that the mass gain trends mainly occurred over Basin 12 (Wilhelm II Land and Queen Mary Land), Basin 13 (Wilkes Land), and the Antarctic Peninsula, at rates of 74.2 ± 8.0 Gt/yr, 63.2 ± 11.6 Gt/yr and 34.1 ± 3.8 Gt/yr respectively. The correlation analysis between the interannual variations of cumulative anomalies in precipitation and total mass suggests that the enhanced precipitation over the coastal EAIS and APIS primarily causes the observed mass gain. Further exploration indicates that the enhanced precipitation is driven by a pair of symmetrically distributed high-pressure systems over the southern ocean surrounding the Antarctic continent, which altered the direction of the prevailing westerly winds and transported more moisture toward the AIS.

Overall, our study continuously monitors the mass change of the AIS for the recent two decades and produces biennial updates of Antarctica's mass change rates in 2021–2022. The assessed biennial mass gain is unusual and offsets the previous contribution to GMSL of 1.3 mm. Our findings emphasize the impact of changing atmospheric circulation on the AIS and hold significant importance for projections of future sea-level rise.

Declaration of Competing Interest

The authors declare that they have no known competing financial interests or personal relationships that could have appeared to influence the work reported in this paper.

CRediT authorship contribution statement

Wei Wang: Conceptualization, Methodology, Software, Validation, Formal analysis, Investigation, Data Curation, Writing - Original Draft, Writing - Review & Editing, Visualization. **Yunzhong Shen:** Methodology, Formal analysis, Investigation, Writing - Review & Editing, Funding acquisition, Supervision. **Qiujie Chen:** Resources, Validation. **Fengwei Wang:**

Investigation, Writing - Review & Editing.

Acknowledgments

We thank the Editor and two anonymous reviewers for their constructive and insightful comments, which helped us considerably improve our manuscript. This work is sponsored by the Natural Science Foundation of China [grant numbers: 42274005, 41974002, 42061134010] and the National Key R&D Program of China [2017YFA0603103]. Dr. Michiel van den Broeke is acknowledged for providing the RACMO2 SMB data.

Data availability

The CSR mascon solutions can be downloaded from: https://www2.csr.utexas.edu/grace/RL06_mascons.html. The MERRA-2 datasets and the ERA reanalysis products are freely accessible online at: https://disc.gsfc.nasa.gov/datasets/M2TMNXFLX_5.12.4/summary and https://www.ecmwf.int/en/forecasts/datasets respectively (Access on 28th April 2023). The RACMO2.3 model can be obtained from: https://doi.org/10.5281/zenodo.7760491 (Access on 1th May 2023). Geopotential and pressure data are obtained from: https://cds.climate.copernicus.eu/cdsapp#!/dataset/reanalysis-era5-pressure-levels-monthly-means?tab=overview(Access on 8th May 2023).

References

A, Geruo, Wahr, J. and Zhong, S. (2013). Computations of the viscoelastic response of a 3-D compressible Earth to surface loading: an application to Glacial Isostatic Adjustment in Antarctica and Canada. *Geophysical Journal International*, 192, 557–572.

Adusumilli, S., Fish, M. A., Fricker, H. A. & Medley, B. (2021). Atmospheric river precipitation contributed to rapid increases in surface height of the west Antarctic ice sheet in 2019. *Geophysical Research Letters*, *48*, 1–11.

Bamber, J. L., Westaway, R. M., Marzeion, B. & Wouters, B. (2018). The land ice contribution to sea level during the satellite era. *Environmental Research Letters*, 13, 063008. https://iopscience.iop.org/article/10.1088/1748-9326/aac2f0

Bars, D. L., Drijfhout, S., & de Vries, H. (2017). A high-end sea level rise probabilistic projection including rapid Antarctic ice sheet mass loss. *Environmental Research Letters*, 12, 044013. https://iopscience.iop.org/article/10.1088/1748-9326/aa6512

Berthier, E., Scambos, T. A., Shuman, C. A. (2012). Mass loss of Larsen B tributary glaciers (Antarctic Peninsula) unabated since 2002. *Geophysical Research Letters, 39*, L13501. https://doi.org/10.1029/2012GL051755

Blanchard-Wrigglesworth, E., Cox, T., Espinosa, Z. I., & Donohoe, A. (2023). The largest ever recorded heat wave characteristics and attribution of the Antarctic heatwave of March 2022. *Geophysical Research Letters*, *50*(17), e2023GL104910. https://doi.org/10.1029/2023GL104910

Bodart, J. A., & Bingham, R. J. (2019). The impact of the extreme 2015–2016 El Niño on the mass balance of the Antarctic ice sheet. *Geophysical Research Letters, 46*, 13, 862–13,871. https://doi.org/10.1029/2019GL084466.

Boening, C., Lebsock, M., Landerer, F., & Stephens, G. (2012). Snowfall-driven mass change on the East Antarctic ice sheet. *Geophysical Research Letters*, *39*, L21501. https://doi.org/10.1029/2012GL053316.

Caron, L., Ivins, E. R., Larour, E., Adhikari, S., Nilsson, J., & Blewitt, G. (2018). GIA model statistics for GRACE hydrology, cryosphere, and ocean science. *Geophysical Research Letters*, *45*, 2203–2212. https://doi.org/10.1002/2017GL076644

Clem, K. R. and M. N. Raphael, Eds., 2022: Antarctica and the Southern Ocean [in "State of the Climate in 2021"]. Bull. Amer. Meteor. Soc., 103 (8), S307–S340, https://doi.org/10.1175/BAMS-D-22-0078.1.

Cogley, J. G. (2012). Area of the ocean. *Marine Geodesy*, *35*(4), 379–388. https://doi.org/10.1080/01490419.2012.709476

Cox, S. C., Smith L. B., Elkind, S., Smith S., C. S., Morin, P., Capponi, G., et al. (2023): The GeoMAP (v.2022-08) continent-wide detailed geological dataset of Antarctica. PANGAEA, https://doi.org/10.1594/PANGAEA.951482

Davison, B. J., Hogg, A. E., Rigby, R., et al. (2023). Sea level rise from West Antarctic mass loss significantly modified by large snowfall anomalies. *Nature Communications, 14*, 1479. https://doi.org/10.1038/s41467-023-36990-3

Diener, T., Sasgen I., Agosta, C, Fürst, J. J., Braun, M. H., Konrad, H. and Fettweis, X. (2021) Acceleration of Dynamic Ice Loss in Antarctica from Satellite Gravimetry. *Frontier in Earth Science*, *9*:741789. https://doi.org/10.3389/feart.2021.741789

Gelaro, R., McCarty, W., Suárez, M. J., Todling, R., Molod, A., Takacs, L., et al. (2017). The modern-era retrospective analysis for research and applications, version 2 (MERRA-2). *Journal of Climate*, *30*(14), 5419–5454. https://doi.org/10.1175/JCLI-D-16-0758.1

González-Herrero, S., Vasallo, F., Bech, J., Gorodetskaya, I., Elvira, B., & Justel, A. (2023). Extreme precipitation records in Antarctica. *International Journal of Climatology*, *43*(7), 3125–3138. https://doi.org/10.1002/joc.8020

Hersbach, H., & Dee, D. (2016). ERA-5 Reanalysis is in production. ECMWF Newsletter, Number 147 (p. 7). Reading, UK: ECMWF.

Ivins, E. R., James, T. S., Wahr, J., Schrama, O., Ernst, J., Landerer, F. W., & Simon, K. M. (2013). Antarctic contribution to sea level rise observed by GRACE with improved GIA correction. *Journal of Geophysical Research: Solid Earth, 118,* 3126–3141. https://doi.org/10. 1002/jgrb.50208.

Khazendar, A, Rignot, E, Schroeder, D. M., Seroussi, H., Schodlok, M. P., Scheuchl, B., Mouginot, J., Sutterley, T. C., Velicogna, I. (2016). Rapid submarine ice melting in the grounding zones of ice shelves in West Antarctica. *Nature Communication*, 7:13243. https://doi.org/10.1038/ncomms13243

Kim B. H., Seo, K. W., Eom, J., Chen, J. L., Wilson, C. R. (2020). Antarctic ice mass variations from 1979 to 2017 driven by anomalous precipitation accumulation. Scientific Reports, 10:20366. https://doi.org/10.1038/s41598-020-77403-5

Li, Z, Chao, B. F., Wang, H.S., Zhang, Z. Z. (2022). Antarctica ice-mass variations on interannual timescale: Coastal Dipole and propagating transports. *Earth and Planetary Science Letters,595*,117789.

Loomis, B. D., Rachlin, K. E., & Luthcke, S. B. (2019). Improved Earth oblateness rate reveals increased ice sheet losses and mass-driven sea level rise. *Geophysical Research Letters, 46,* 6910–6917. https://doi.org/10.1029/2019GL082929

Loomis, B. D., Rachlin, K. E., Wiese, D. N., Landerer, F. W., & Luthcke, S. B. (2020). Replacing GRACE/GRACE-FO C30 with satellite laser ranging: Impacts on Antarctic Ice Sheet mass change. *Geophysical Research Letters, 47*, e2019GL085488. https://doi.org/10.1029/2019GL085488

Mouginot, J., Rignot, E., Scheuchl, B. (2014). Sustained increase in ice discharge from the Amundsen Sea Embayment, West Antarctica, from1973 to 2013. *Geophysical Research Letters,* 41:1576–1584. https://doi.org/10. 1002/2013GL059069

Mouginot, J., B. Scheuchl, and E. Rignot. (2017). MEaSUREs Antarctic Boundaries for IPY 2007-2009 from Satellite Radar, Version 2. [Indicate subset used]. Boulder, Colorado USA. NASA National Snow and Ice Data Center Distributed Active Archive Center. https://doi.org/10.5067/AXE4121732AD. [Date Accessed].

Oppenheimer, M., B.C. Glavovic, J. Hinkel, R. van de Wal, A.K. Magnan, A. Abd-Elgawad, R. Cai, M. Cifuentes-Jara, R.M. DeConto, T. Ghosh, J. Hay, F. Isla, B. Marzeion, B. Meyssignac, and Z. Sebesvari, (2019): Sea Level Rise and Implications for Low-Lying Islands, Coasts and Communities. In: IPCC Special Report on the Ocean and Cryosphere in a Changing Climate [H.-O. Pörtner, D.C. Roberts, V. Masson-Delmotte, P. Zhai, M. Tignor, E. Poloczanska, K. Mintenbeck, A. Alegría, M. Nicolai, A. Okem, J. Petzold, B. Rama, N.M. Weyer (eds.)]. Cambridge University Press, Cambridge, UK and New York, NY, USA, pp. 321–445. https://doi.org/10.1017/9781009157964.006.

Otosaka, I. N., Shepherd, A., Ivins, E. R., Schlegel, N.-J., Amory, C., van den Broeke, M. R.et al. (2022). Mass Balance of the Greenland and Antarctic Ice Sheets from 1992 to 2020. *Earth System Science Data,* https://doi.org/10.5194/essd-2022-261.

Otosaka, I. N., Horwath, M., Mottram, R., Nowicki, S. (2023). Mass Balances of the Antarctic and Greenland Ice Sheets Monitored from Space. *Surveys in Geophysics,* https://doi.org/10.1007/s10712-023-09795-8

Peltier, W. R., D. F. Argus, and R. Drummond. (2018). Comment on "An assessment of the ICE-6G_C (VM5a) glacial isostatic adjustment model" Purcell et al., *J. Geophys. Res. Solid Earth*, 123, 2019–2028. https://doi.org/10.1002/2016JB013844

Rignot, E, Mouginot, J, Morlighem, M, Seroussi, H, Scheuchl, B. (2014). Widespread, rapid grounding line retreat of Pine Island, Thwaites, Smith, and Kohler glaciers, West Antarctica, from 1992 to 2011. *Geophysical Research Letters,* 41, 3502–3509. https://doi.org/10.1002/2014GL060140

Rignot, E., Mouginot, J., Scheuchl, B., Van den Broeke, M., van Wessem, M. J., and Morlighem, M. (2019). Four Decades of Antarctic Ice Sheet Mass Balance from 1979-2017. *Proc. Natl. Acad. Sci.,* 116, 1095–1103. https://doi.org/10.1073/pnas.1812883116.

Sasgen, I., Wouters, B., Gardner, A. S., King, M. D., Tedesco, M., Landerer, F. W., et al. (2020). Return to rapid ice loss in Greenland and record loss in 2019 detected by the GRACE-FO satellites. Communications Earth & Environment, 1–8. https://doi.org/10.1038/s43247-020-0010-1

Sasgen, I., Martín-Español, A., Horvath, A., Klemann, V., Petrie, E. J., Wouters, B. et al. (2018). Altimetry, gravimetry, GPS and viscoelastic modeling data for the joint inversion for glacial isostatic adjustment in Antarctica (ESA STSE Project REGINA). *Earth System Science Data*, 10, 493–523.

Save, H., Bettadpur, S., Tapley, B.D., 2016. High-resolution CSR GRACE RL05 mascons. *Journal of Geophysical Research: Solid Earth, 121* (10), 7547–7569.

Save, H., 2020. CSR GRACE and GRACE-FO RL06 Mascon Solutions v02. University of Texas. https://doi.org/10.15781/cgq9-nh24 [data set].

Schröder, L., Horwath, M., Dietrich, R., Helm, V., van den Broeke, M. R., and Ligtenberg, S. R. M. (2019). Four decades of Antarctic surface elevation changes from multi-mission satellite altimetry. *The Cryosphere*, 13, 427–449. https://doi.org/10.5194/tc-13-427-2019

The IMBIE team. (2018). Mass balance of the Antarctic Ice Sheet from 1992 to 2017. *Nature*, 558, 219–222.

Shepherd, A., Gilbert, L., Muir, A. S., Konrad, H., McMillan, M., Slater, T., et al. (2019). Trends in Antarctic Ice Sheet elevation and mass. *Geophys. Res. Lett., 46*, 8174–8183. https:// doi.org/10.1029/2019GL082182

Smith, B., Fricker, H. A., Gardner, A. S., Medley, B., Nilsson, J., Paolo, F. S., et al. (2020). Pervasive ice sheet mass loss reflects competing ocean and atmosphere processes. *Science*, 368, 1239–1242. https://doi.org/10.1126/science.aaz5845

van Wessem, J. M., Jan Van De Berg, W., Noël, B. P., Van Meijgaard, E., Amory, C., Birnbaum, G., et al. (2018). Modelling the climate and surface mass balance of polar ice sheets using RACMO2: Part 2: Antarctica (1979–2016). *The Cryosphere*, *12*(4), 1479–1498.

Velicogna, I., T. C. Sutterley, and M. R. van den Broeke. (2014). Regional acceleration in ice mass loss from Greenland and Antarctica using GRACE time-variable gravity data, *Geophysical Research Letters*, *41*, 8130–8137. https://doi.org/10.1002/2014GL061052.

Velicogna, I., Mohajerani, Y., A, G., Landerer, F., Mouginot, J., Noel, B., et al. (2020). Continuity of ice sheet mass loss in Greenland and Antarctica from the GRACE and GRACE Follow-On missions. *Geophysical Research Letters*, *47*, e2020GL087291. https://doi.org/10.1029/2020GL087291.

Whitehouse, P. L., Bentley, M. J., Milne, G. A., King, M. A., and Thomas, I. D. (2012). A new glacial isostatic adjustment model for Antarctica: calibrated and tested using observations of relative sea-level change and present-day uplift rates. *Geophysical Journal International*, 190, 1464–1482.

Wille, J. and the East Antarctica heatwave project: The extraordinary March 2022 East Antarctica heatwave, EGU General Assembly 2023, Vienna, Austria, 24–28 Apr 2023, EGU23-8107, https://doi.org/10.5194/egusphere-egu23-8107, 2023.

Yue, L., Chao, N., Chen, G., Chen, L., Zhang, B., Sun, R., et al. (2023). Reconstructing continuous ice sheet elevation changes in the Amundsen Sea sector during 2003–2021 by merging Envisat, ICESat, CryoSat-2, and ICESat-2 multi-altimeter observations. *Journal of Geophysical Research: Earth Surface*, 128, e2022JF007020. https://doi.org/10.1029/2022JF007020

Zhang, B., Liu, L., Yao, Y., van Dam, T., Khan, S. A. (2020). Improving the estimate of the secular variation of Greenland ice mass in the recent decades by incorporating a stochastic process. *Earth and Planetary Science Letters, 549,* 116518.

Zwally, H. Jay, Mario B. Giovinetto, Matthew A. Beckley, and Jack L. Saba, 2012, Antarctic and Greenland Drainage Systems, GSFC Cryospheric Sciences Laboratory, at http://icesat4.gsfc.nasa.gov/cryo_data/ant_grn_drainage_systems.php